ASIAN JOURNAL OF PHARMACEUTICAL AND CLINICAL RESEARCH

INNOVARE ACADEMIC SCIENCES
Knowledge to Innovation

Vol 19, Issue 1, 2026

Online - 2455-3891
Print - 0974-2441

Research Article

GREEN SYNTHESIS OF CHITOSAN-MEDIATED SILVER NANOCOMPOSITE USING *PIPER BETEL* STEM EXTRACT: EVALUATING ANTIBACTERIAL AND ANTICANCER ACTIVITY

KODIGANTI NARESH KUMAR[1], NALINI DEVARAJAN[1]*, PAVITHRA AMRITKUMAR[1], THARANI MUNUSAMY[1], MALCHI SURESH[1], MANJU BARGAVI S[2]

[1]Department of Research, Meenakshi Academy of Higher Education and Research, K. K. Nagar, Chennai, Tamil Nadu, India. [2]Department of Nutrition and Dietetics, Faculty of Humanities and Science, Meenakshi Academy of Higher Education and Research, Chennai, Tamil Nadu, India.

***Corresponding author: Nalini Devarajan; Email: drnalini.crl@madch.edu.in**

Received: 12 August 2025, Revised and Accepted: 28 October 2025

ABSTRACT

Objective: The integration of herb-based nanomedicine has gained significant attention, aiming to improve therapeutic outcomes while minimizing drug toxicity. *Piper betel* is a medicinal herb widely used in traditional therapy due to its potent anticancer, antimicrobial, antioxidant, and anti-inflammatory properties.

Methods: *P. betel* stem extract is used to synthesize chitosan-mediated silver nanocomposite (AgNC). Characterization was done using UV-visible spectrophotometry, Fourier transform infrared (FTIR), X-ray diffraction, dynamic light scattering with Zeta potential, and FESEM with energy dispersive X-ray. Its antibacterial activity was evaluated in *Staphylococcus aureus, Pseudomonas aeruginosa*, and *Escherichia coli*, as well as antioxidant diphenyl-2-picrylhydrazyl and anti-inflammatory assays (egg albumin and bovine serum albumin) were performed. Further, its anticancer activity was evaluated in A549 and Henrietta Lacks (HeLa) cell lines.

Results: AgNC exhibited a sharp surface plasmon resonance peak at 450 nm. FTIR analysis revealed various peaks. Scanning electron microscopy analysis revealed a soft-fibrous sheet-like morphology. In antibacterial activity, a significant zone of inhibition was observed against *P. aeruginosa* and *E. coli* (16 mm). In addition, AgNC exhibited inhibition of free radicals and protein denaturation. In anticancer activity, it showed greater activity against A549 (66.7±5.9 µg/mL) than HeLa (85.7±7.8 µg/mL), and reduced cell migration within 48 h at 80 µg/mL in A549 cell lines.

Conclusion: These findings highlight AgNCs as the most promising candidates for biomedical applications, particularly for antibacterial and anticancer therapy. However, further investigations are required to elucidate the precise molecular mechanisms of therapeutic efficacies and modifications to enhance their anticancer activity.

Keywords: Green synthesis, Chitosan, Silver nanocomposite, *Piper betel* stem, Anticancer, Antibacterial.

 DOI: http://dx.doi.org/10.22159/ajpcr.2026v19i1.56502. Journal homepage: https://innovareacademics.in/journals/index.php/ajpcr

INTRODUCTION

Nanotechnology has become an innovative approach in biomedical applications in recent years, providing improved efficacy in the treatment of disease and drug delivery [1]. Recently, the medical sector has expressed greater interest in herbal medicines to achieve sustainable activity and less toxicity of drugs [2]. Among the several nanomaterials, silver nanoparticles (AgNPs) have gathered significant attention due to their broad-spectrum antimicrobial properties and promising applications in cancer therapeutics [3]. Conventionally, chemical and physical methods have been employed to synthesize AgNPs; however, these methods often involve toxic reagents, expensive processes, and hazardous by-products. As a sustainable alternative, green synthesis has gained attraction, leveraging natural plant extracts as reducing and stabilizing agents to minimize environmental impact [4]. The use of plant-based extracts in nanomaterial synthesis offers several advantages, such as biocompatibility, cost-effectiveness, and the presence of bioactive phytochemicals that enhance the therapeutic potential of the synthesized nanomaterials [5].

Piper betel is an evergreen dioecious plant commonly grown throughout India. It belongs to the family of *Piperaceae*, also known as Paan in India and other subcontinental nations. It is a well-known medicinal plant that demonstrated a wealth of bioactive compounds (β-caryophyllene, eugenol, hydroxychavicol, estragole, caryophyllene,1,8-cineol, α-pinene, β-pinene, and hydroxy catechol), which exhibit antimicrobial, antifungal, anticancer, antioxidant, and anti-inflammatory activity [6]. These phytochemicals (alkaloids, flavonoids, coumarins, tannins, terpenoids, cardiac glycosides, and saponins), chief components, chavibetol, chavicol, and polyols, enhance capping and reducing nature, making *P. betel* an excellent source for the green synthesis of NPs [7].

Chitosan can be used with silver (Ag) NPs to enhance its antibacterial and anticancer activity [5,8]. Chitosan interacts with nanometals to produce nanocomposites. These delivery methods span from microparticles to NPs, composites, nano-fibers, and films. Metallic NPs with chitosan improve the release of loaded anticancer medications, allowing sustained release, lowering the required dose, and minimizing harm to healthy cells [9]. Chitosan produced from crustacean animal shell waste has been widely used as an antifungal, medicinal coating, wound healing, and antioxidant [10]. The benefits of chitosan were that it is nontoxic, cheap, biocompatible, degradable, and water-soluble. It has been used in drug delivery, advanced cancer therapy [11]. Chitosan NPs (CNPs) are promising versatile cationic polymeric NPs, due to their incredibly tiny size; CNPs have fascinating interaction and surface properties. It showed effective antimicrobial activity against the pathogens *Escherichia coli, Pseudomonas aeruginosa*, *Klebsiella pneumonia,* and *Staphylococcus aureus* [12,13].

Cancer is one of the life-threatening and leading causes of death. It can affect various organs and tissues, leading to severe health complications and high mortality rates [14]. Traditional treatments for cancer, such as

chemotherapy, radiation therapy, and surgery, are expensive procedures and also often come with side effects, including toxicity to healthy cells, drug intolerance, and drug resistance in a few patients [15]. Due to these drawbacks, continuous research is being conducted to explore natural, inexpensive, anti-proliferative, and chemopreventive agents as alternatives to synthetic drugs, mainly aiming to achieve lower toxicity with fewer side effects [16,17]. Ultrafine NPs were created using green methods, which is an essential property for a variety of applications where a particular surface area is important [11].

This research demonstrates a sustainable and efficient method for creating silver nanocomposites using an environmentally friendly approach, involving *P. betel* stem extract and chitosan [18]. Their physicochemical properties and biological activities were evaluated with an emphasis on determining their anticancer efficacy against Henrietta Lacks (HeLa), A549, and Human Embryonic Kidney (HEK) cell lines. Their antibacterial potential against pathogenic bacterium (*S. aureus, P. aeruginosa*, and *E. coli*).

Hypothesis of the study

We hypothesized that a chitosan-silver nano composite (Chitosan-AgNC) made using *P. betel* stem extract would exhibit antibacterial and anticancer properties.

Study objectives

1. To synthesize and characterize Chitosan-AgNC using *P. betel* stem aqueous extract
2. To evaluate the antibacterial activity of Chitosan-AgNC against *E. coli* and *P. aeruginosa,* and S. *aureus* using agar well diffusion, cytoplasmic leakage, protein leakage, and antibiofilm assays
3. To assess the *in vitro* anticancer potential of Chitosan-AgNC against A549 and HeLa cell lines using 3-(4,5dimethylthiazol-2-yl)-2,5-diphenyltetrazolium bromide (MTT) and cell migration assays in the A549 cell line.

MATERIALS AND METHODS

Materials

HeLa cervical cancer cell line, A549 (Human lung cancer), and HEK cell lines were procured from the National Centre for Cell Sciences, Pune, India. Dulbecco's modified Eagle's medium (DMEM) (DMEM, Cat; 11995065, Gibco), Fetal bovine serum (FBS) (FBS: Cat; 26140095, Gibco, US), 1% penicillin–streptomycin (P4333, Sigma-Aldrich, St. Louis, MO, USA), 0.5% Trypsin-Ethylenediaminetetraacetic acid (EDTA) (Cat; 15400054, Gibco), CyQUAN TMTT reagent (Cat; V13154, Invitrogen, Thermo Fisher Scientific, USA). For anti-bacterial assays, Nutrient agar, Muller–Hinton agar, and BHI broth were purchased from HiMedia Laboratories Private Limited, India. Amoxicillin (Alkem Laboratories) was used as a standard drug for anti-bacterial assays, and diclofenac for anti-inflammatory assays.

Instruments/equipment

Ultraviolet (UV-visible) spectrophotometer (Shimadzu UV-1900i, Shimadzu Corporation, Japan), Fourier transform infrared (FTIR) (Spectrum-2, PerkinElmer, Singapore), X-ray diffraction (XRD) (ARL EQUINOX 3000, Thermo Fisher Scientific, USA), dynamic light scattering (DLS) with Zeta potential (Malvern Zetasizer, Massachusetts, US), Field emission scanning electron microscopy (FESEM) images with energy dispersive X-ray spectroscopy (EDX) Scanning Electron Microscope (ZEISS, Gemini 1, Sigma 300, Germany), Enzyme-Linked Immunosorbent Assay reader (iMark**,** Bio-Rad, Japan), Inverted Microscope (EXI-310 Trinocular with FL Illuminator-3, Accu-scope, NY, USA), CO_2 incubator (Hera Cell Vios160i LK, Thermo Scientific, Germany), Digital Antibiotic Zone reader (1941, Electronics, Haryana, India), and Centrifuge (Sorvall ST 8R, ThermoScientific, Germany).

Collection of plant and authentication

Fresh *P. betel* plant (Fig. 1) was collected from Annaji Nagar Park, 2nd Main Road, (GPS coordinates: 13°02'26.2"N 80°11'20.3"E), KK Nagar, Chennai, India. The authentication was done by the Central Council for Research in Siddha (Voucher specimen Code: P31082404B, and Botanical name: *Piper betle* L.), Ministry of AYUSH, Anna Government Hospital Campus, Arumbakkam, Chennai, India.

Preparation of aqueous extract

The plant was rinsed thoroughly with distilled water, and the stem was separated from the plant and then cut into small pieces [19]. These finely cut pieces were dried at room temperature for 2 weeks, then transferred to a hot air oven at 37°C for 3 days. Then, the dried stem was powdered using a mortar and pestle. This fine powder was stored in an airtight container at room temperature for further use.

1% aqueous extract was prepared by dissolving 1 g of the above-mentioned dry powder in 100 mL of double-distilled water and boiling for 30 min at 60°C using a magnetic stirrer [20]. The extract was filtered through Whatman Filter paper no. 1. This filtrate was utilized for AgNP synthesis.

Synthesis of AgNPs

20 mL of *P. betel* stem filtered aqueous extract was added dropwise to 0.01M $AgNO_3$ solution and subjected to stirring for 20 min, resulting in the formation of colloidal nano-silver [21]. Then, it was transferred to an orbital shaker at 37°C. The transition in color indicates the formation of NPs.

Synthesis of Ag-nano composite

Preparation of 1% (w/v) chitosan solution

To prepare 1% chitosan solution, 0.5 g of chitosan powder was dissolved in 9 mL of Distilled water. To facilitate the degradation of chitosan, 1 mL of 85% (v/v) glacial acetic acid was added to the mixture [22]. Then, this solution was stirred thoroughly at 800 rpm for 5 h to achieve a homogeneous mixture.

Preparation of chitosan-mediated silver nanocomposite (AgNC)

Equal volumes of the prepared *P. betel* stem AgNPs solution and 1% chitosan solution were mixed in a 1:1 ratio [23]. It was stirred using a magnetic stirrer for 30 min. Then, transferred to an orbital shaker for 48 h for composite formation. The resulting nanocomposite (AgNC) was collected by centrifugation at 8,000 rpm for 10 min [12,24]. The pellet was collected and washed with distilled water several times, and the obtained product was heated at 70°C for 6 h [25]. The powder was used for further processing.

Characterization of AgNC

The formation of AgNPs and AgNP-chitosan composite (AgNC) was primarily confirmed by measuring λ max with a UV-visible spectrophotometer wavelength range between 200 and 700 nm [2]. The functional groups were determined by FTIR spectroscopy, crystalline structure was performed using XRD, particle size and surface charge were determined using DLS and Zeta potential [11]. The shape and surface morphology were investigated using Scanning Electron Microscopy (SEM) FESEM. Elemental analysis was done using EDX.

Antibacterial activity

The antibacterial potential of AgNC was evaluated by the Agar well-diffusion method against *S. aureus, P. aeruginosa, and E. coli*. The MHA plate surface was inoculated with bacterial culture by spreading microbial inoculum over the entire media. Then, 4 wells were created using a sterile 1 mL pipette tip, each well labeled with a concentration of AgNC and standard amoxicillin. 25, 50, and 100 µg of AgNC, standard drug loaded into the wells, left for incubation at 37°C for 24 h, and evaluated for zone of inhibition by measuring zone around the well using antibiotic zone reader [8,26].

Minimum inhibitory concentration (MIC) and minimum bactericidal activity (MBC)

The bacterial organisms were inoculated in Nutrient broth overnight, then diluted with 0.85% sterile saline in BHI broth to get 0.5

McFarland's standard (1×10^5 Colony Forming Units/mL). Then, the incubation was continued for 4 h at 37°C, and broth, diluted with AgNC from 0.5 to 50 µg/mL (0.5, 1, 5, 10, 15, 20, 25, 30, 35, 40, 45, 50 µg/mL). The negative control (−) was carried out with sterile broth, whilst the positive control (+) remained untreated. Finally, microtubes were incubated at 37°C for 24 h. The lowest concentration with no apparent turbidity was identified as the MIC. The MBC was calculated by subculturing the MIC tube onto nutrient agar and observing the absence of bacterial colonies following an overnight incubation [27].

Cytoplasmic leakage assay

Bacterial strains were cultured in BHI broth and incubated overnight at 37°C in an orbital shaker [28]. Then, the culture was exposed to different concentrations of AgNC (25, 50, 100 µg/mL) and standard drug (amoxicillin) for 24 h, then the supernatant was collected by centrifugation at 6,000 rpm for 15 min, and analyzed spectrophotometrically at 595nm.

Protein leakage assay

Barford assay was performed to analyze the protein leakage by bacterial cells [29]. The *S. aureus*, *P. aeruginosa, and E. coli* were cultured in BHI broth for 24 h. Each organism was treated with 25 µL of 25, 50, and 100 µg/mL of AgNC and the standard drug in 1 mL of cultured broth, incubated at 37°C for 12 h. After treatment, the tubes were centrifuged at 6,000 rpm for 15 min, and the supernatant was collected. For each sample, 25 µL of the supernatant was mixed with 200 µL of reagent and kept in the dark for 30 min. The absorbance was measured at 595 nm.

Antioxidant assay

Diphenyl-2-picrylhydrazyl (DPPH)

The antioxidant property of AgNC was evaluated using the DPPH protocol by Dhanraj and Rajeshkumar 2021 with slight modification [3,30]. To prepare 0.1 mm DPPH reagent, 4 mg of DPPH was dissolved in 100 mL of 100% Methanol to make a stock solution. 100 µL of 25, 50, and 100 µg/mL AgNC were added to 3 mL of DPPH solution. The reaction mixture was incubated at room temperature in dark conditions for 20 min. The absorbance of each sample was measured at 517 nm using a UV-vis spectrophotometer. Ascorbic acid was used as a standard. % of radical scavenging activity (RSA) calculated using below formula.

$$\text{Percentage of RSA} = \frac{\text{Abs of control} - \text{Abs of sample}}{\text{Abs of control}} \times 100$$

Anti-inflammatory assay

Bovine serum albumin (BSA) denaturation assay

A heat-induced protein denaturation assay was carried out to evaluate the anti-inflammatory activity described by Chandra *et al*. 2012 with minor modifications [31]. 100 µL various concentrations of AgNC (25, 50, 100 µg/mL), standard drug diclofenac sodium added to 1 mL of 1% BSA in phosphate-buffered saline (PBS) (pH 6.4), incubated at 37°C for 20 min, then the samples were shifted to a water bath at 70°C for 5min. Turbidity was measured at 660 nm after the cooling samples. The % inhibition of BSA denaturation was calculated using the following formula:

$$\text{Inhibition of protein denaturation } (\%) = \frac{\text{Abs of control} - \text{Abs of sample}}{\text{Abs of control}} \times 100$$

Egg albumin (EA) denaturation assay

An EA denaturation assay was performed to evaluate the anti-inflammatory activity of AgNC described by Ameena *et al*., in 2023 [32]. 0.2 mL of 1% freshly prepared EA mixed with 2.8 mL of 1×PBS (pH 6.4), 2 mL of different concentrations of AgNC (25, 50, 100 µg/mL), and 2 mL of diclofenac sodium (positive control) mixed well and incubated at 37°C for 15 min. Then, it was shifted to a water bath to heat at 70°C for an additional 5 min to induce denaturation. The absorbance of denaturation was measured at 660 nm using a UV-visible spectrophotometer. The % inhibition of EA denaturation was calculated using the above formula.

Antibiofilm activity

Anti-biofilm activity of AgNC tested by crystal violet assay. *S. aureus*, *P. aeruginosa, and E. coli* colonies were inoculated in BHI broth and incubated in an orbital shaker at 37°C overnight. 200 µL culture incubated with different concentrations of AgNC in designated wells, and amoxicillin was used as a Standard in 96-well plates, incubated for 48 h at 28°C. The formed biofilm was washed 3 times using 1×PBS, fixation was done using methanol for 15 min, and stained with 0.1% crystal violet for 30 min; unbound stain was rinsed with distilled water 3–4 times. Biofilm solubilized in ethanol and acetone (1:9). The optical density was measured using a microplate reader at 590 nm [29,33].

Anticancer activity

Cell culture

A549, HeLa, and HEK cell lines were supplemented with DMEM high glucose, 10% FBS, and 1% penicillin-streptomycin, and cultured in a CO_2 incubator with 5% CO_2 and 95% humidity at 37°C. The cells were sub-cultured after reaching 70% confluence by detaching cells using

Fig. 1: *Piper betel* plant

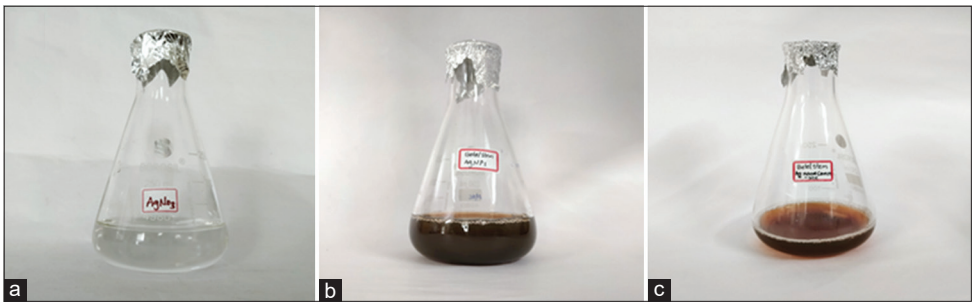

Fig. 2: Visual observation of silver nanoparticles synthesis (a) $AgNO_3$ solution, (b) color change on the addition of piper betel stem aqueous extract, (c) silver nanoparticles with 1% chitosan

0.5% Trypsin-EDTA, and then the trypsin activity was deactivated by adding double the volume of complete medium.

Cell cytotoxicity (MTT)

Cell proliferation was quantified using the CyQUANT MTT reagent (Thermos Fisher), according to the protocol provided in product sheet [34]. The cells were seeded in 96-well plate (1×10^4 cells/well) and incubated to adhere the cells, then treated with cisplatin and AgNC (0, 10, 20, 40, 60, 80, 100, 200 µg/mL) for 24 h [35]. Upon treatment, the plates were replaced with 100 µL of fresh media without phenol red indicator and incubated for another 4 h by adding 10 µL MTT reagent per well. 100 µL of SDS-HCL solution was added to each well mixed using a pipette, and incubated for 4–8 h. The absorbance was recorded at 570 nm. The viability percentage was calculated using the below formula,

$$\text{Percentage of cell viability} = \frac{\text{Abs of treated}}{\text{Abs of control}} \times 100$$

Cell migration assay

A stretch wound healing assay was done in A549 cell lines to assess Cell migration [36]. After getting 70% confluence, cells were seeded (2×10^5/well) into a 6-well plate and cultured monolayer, and the wound was created in the middle of the plate using a sterile 200 µL tip. Removed cell debris by washing with PBS and treated with AgNC (0, 20, 40, 80, 100 µg/mL) in complete media. Photos were captured at different time points (0, 24, and 48 h). The wound distance was evaluated using CaptaVision+™ software (Accu-Scope, EXI- 310-FL3, USA). The percentage of wound closure is calculated using the formula;

$$\%\ \text{of Wound closure} = \frac{W0 - Wt}{W0} X100$$

W0: Initial wound area; Wt: Wound area after treatment at different time points.

Statistical analysis

All experiments were done in triplicate (n=3), and the data were analyzed by Two-way Analysis of Variance, followed by the difference between groups determined using Tukey multiple comparisons, and a Student's t-test used for two-group comparison. All statistical analysis was done using Prism GraphPad software version 10.4.1 (Windows). The data are presented as mean±standard error. Moreover, statistical significance is represented in asterisks (*),*p<0.05, **p<0.01, ***p<0.001, ****p<0.0001, and ns indicates a p>0.05 statistically not significant.

RESULTS AND DISCUSSION

Visual observation of NP formation

The formation of brown color was observed on addition of *P. betel* stem extract in 1 mm $AgNO_3$ within 3 h, and the intensity of color strengthened during 24–48 h incubation (Fig. 2b) [37]. When it was mixed with Chitosan, it turned a light Greyish (Fig. 2c) [21]. Due to the presence of phytochemicals such as flavonoids, phenols, and alkaloids, they act as reducing and stabilizing agents [7]. Similar results were observed by Kanniah *et al*. in silver nanocomposite synthesis using *Piper nigrum* seed extract [4].

UV-vis spectrophotometer

The UV spectrum analysis of AgNPs synthesized from betel stem showed a maximum absorption peak at 450nmand declined absorption at higher wavelengths (Fig 3a). Indicating the presence of surface plasmon resonance of AgNPs and their formation [38,39]. The absorption spectrum analysis of AgNPs of betel stem extract on the addition of 1% Chitosan at 1 h slightly decreased in absorbance, indicating initial formation, at 18, 24, and 36 h further decrease in absorption indicates continued stabilization and possible changes in betel stem extract AgNPs with chitosan (Fig. 3b). This behavior aligns with the findings by (Arif *et al*.,) [24], who reported similar trends in the interaction of AgNPs with stabilizing agents.

FTIR

The functional group's analysis of chitosan-based silver NP (AgNC) synthesized from betel stem extract exhibited major absorbance peaks at different wavelengths, indicating the presence of hydroxyl, amine groups, amide II, aliphatic chain, hydrocarbons, glycosidic, and metal-oxide bonds (Fig. 4). The broad peak at 3,255 cm^{-1} corresponds to OH or NH functional groups and the role of chitosan as a reducing and stabilizing agent, as reported in the literature [40,41] in the synthesis of metal NPs. The peak at 1,544 cm^{-1} and 1,535 cm^{-1} related to N-H bending vibrations supports the involvement of amine groups in NP stabilization [39]. The peak at 1,403 cm^{-1} corresponds to C-H binding vibrations, 1,013 cm^{-1} I associated with glycosidic (C-O-C) bonds. Various peaks in a range between 400 and 700 cm^{-1} attributed to metal-oxygen bonds indicate AgNP interaction with chitosan [5,8]. These results suggest the effective reduction and stabilization of AgNPs with chitosan.

XRD analysis

The crystalline nature of synthesized AgNPs and Ag-chitosan nanocomposite (AgNC) were characterized by XRD, and the resulting diffraction pattern is shown in Fig. 5. The AgNPs exhibited peaks at 2θ=38.28°, 44.25°, 64.46°, 77.60°, and 87.52°, corresponding to the planes of face-centered cubic (FCC) silver. The intense reflection at 38.15° indicates high crystallinity of AgNPs [42]. For AgNC diffraction peaks were observed at 2θ=21.56°, 38.06°, 44.25°, 64.54°, 77.55°, and 87.73°. The broad peak centered around 21.56° corresponds to the semi-crystalline nature of chitosan, arising from the regular arrangement of polymeric chains. The distinct peaks appearing at 38.06°, 44.25°, 64.54°, and 77.55° are characteristic of FCC silver (Ag), and an additional weak peak at 87.73° may correspond to the metallic silver, confirming the successful formation of crystalline AgNPs within the chitosan matrix. These results were aligned with the previous

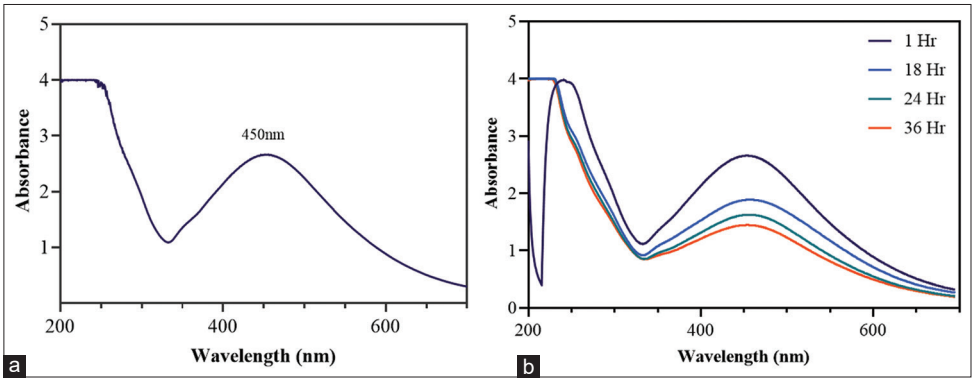

Fig. 3: Ultraviolet-visible spectrophotometer analysis of (a) silver nanoparticles, (b) silver nanocomposite

research done by Kalaivani *et al*. in 2018 and Mannopantar *et al*. in 2022 [11,40,43].

DLS and zeta potential

The successful green production and surface modification of AgNPs using chitosan and *P. betel* stem extract is confirmed by the DLS and Zeta potential studies at temperature 25ºC (Fig. 6). The AgNPs exhibited an average size of 138.8 nm and Zeta potential of −38.6 mV, while the silver nano composite (AgNC) displayed a large size 244 nm and higher negative surface charge −61.1 mV with polydispersity index (PDI)=0.403, these increase in particle size attributes the formation of chitosan coating layer, and the higher zeta potential indicates greater electrostatic stability (Tables 1 and 2), these results were correlated with Jalab *et al*. in 2021 the particle size and PDI was depends on concentration of extract and silver nitrate ratio [44].

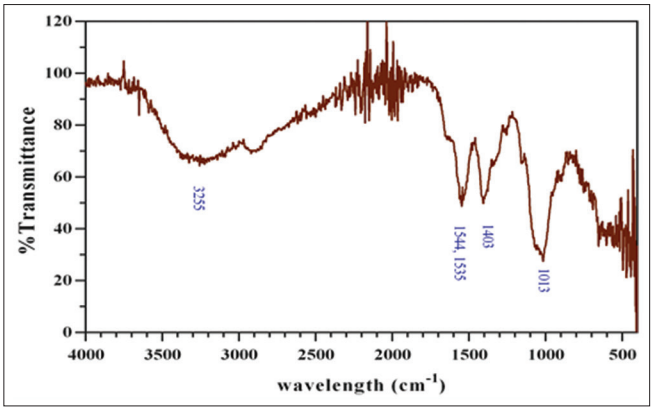

Fig. 4: Fourier transform-infrared spectrum graph of silver nanocomposite, functional groups analysis

The low PDI (0.218) in nanocomposite supports enhanced homogeneity, colloidal stability, and a fairly monodispersed. The findings support *P. betel* stem extract efficacy as a bio-reductant and stabilizer, and chitosan as a biopolymer coating agent, which form stable AgNC with prospects of application in antimicrobial and biomedical fields [43,45].

Morphological assessment (SEM)

SEM imaging was used to investigate the morphology of AgNC at various magnifications, revealing distinct structural features. At lower magnification 10 µm, a layered non-homogeneous, non-smooth morphology with parallel ridges indicates structural alignment and possible integration of NPs (Fig. 7a) [4,39]. At 2 µm, the surface morphology with rough and porous structures in the micron range (Fig.7b) [18]. In higher magnification at 500 nm, it shows smooth, compact layers of closely packed structures, representing a chitosan

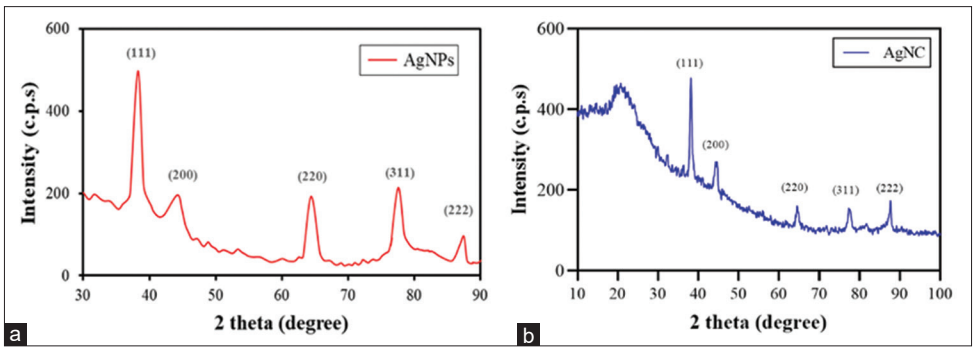

Fig. 5: X-ray diffraction pattern of (a) silver nanoparticles, and (b) Ag-chitosan nanocomposite (silver nanocomposite) showing characteristic diffraction peaks of crystalline silver planes on the semi-crystalline chitosan background in silver nanocomposite

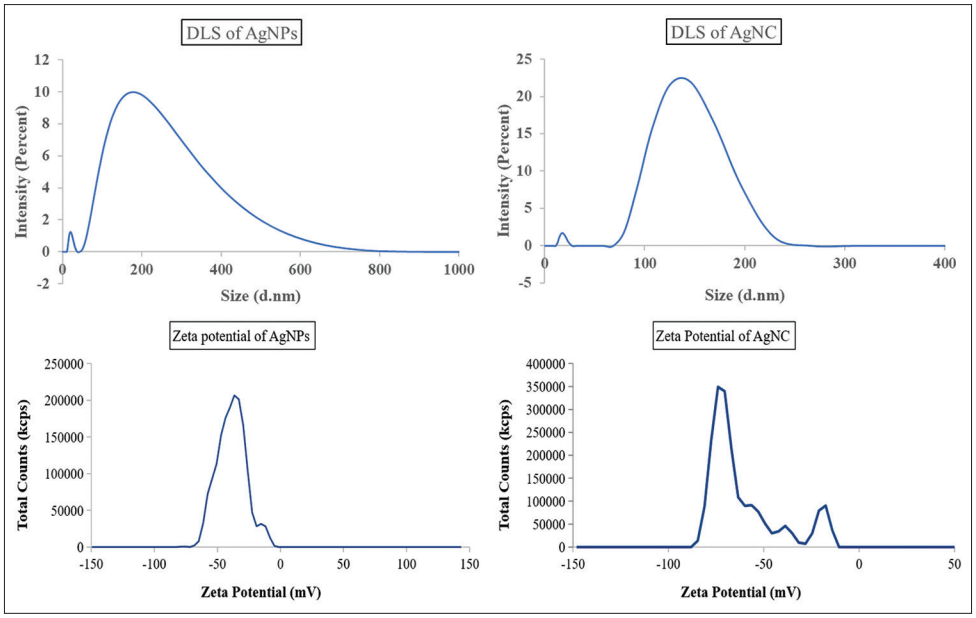

Fig. 6: Dynamic light scattering intensity and Zeta potential distribution of silver nanoparticles and Ag-Chitosan nanocomposite (silver nanocomposite) showing enhanced colloidal stability after surface modification

matrix (Fig. 7c-d) with AgNPs [13]. These features of roughness and porosity indicate the successful incorporation of AgNPs with chitosan, enhancing drug-releasing efficiency.

Elements analysis EDX

The EDX spectrum revealed a Stronge signal of silver (Ag) along with characteristic peaks of carbon (C) and oxygen (O), as well as minor peaks of Na, AI, Si, Cl, K, Ca, Fe, and Cu (Fig. 8a). The high carbon (44.26%) and oxygen (32.33%) corresponding to the chitosan polymeric framework and phytochemical capping agents derived from *P. betel* stem extract, as well as the prominent Ag peak, which confirmed the successful synthesis and presence of AgNP in the nanocomposite matrix (Fig. 8b and Table 3), accounting for 12.79%. These results are consistent with DLS and zeta potential studies, indicating that the nanocomposite is constituted of both metallic and biopolymeric phases, is well disseminated, and is chemically stable. The presence of Ag confirms NP formation, while C and O indicate involvement of chitosan and *Pipet betel* stem extract in the formation of the organic matrix.

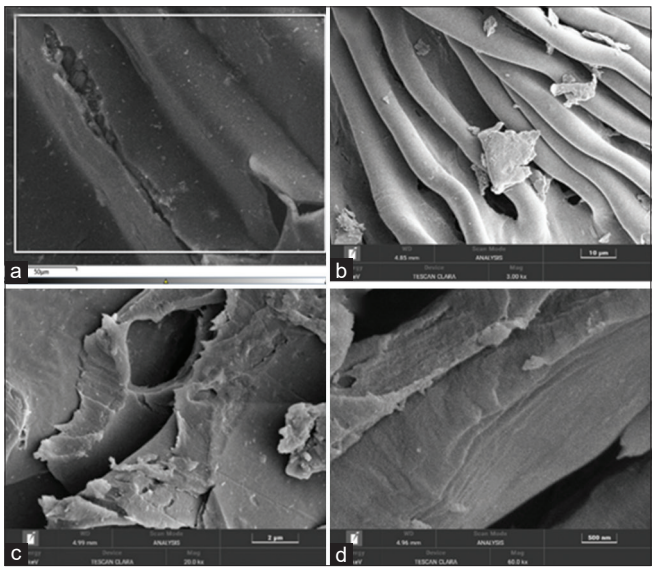

Fig. 7: Scanning electron microscopy images of silver nanocomposite; (a) 50 μm, (b) 10 μm, (c) 2 μm, (d) 500 nm

Antibacterial assay

The AgNC exhibited concentration-dependent antibacterial activity against *S. aureus*, *P. aeruginosa*, and *E. coli* at concentrations of 25, 50,

Table 1: DLS parameters of AgNPs and AgNC nanocomposite

Parameter	AgNPs (silver nanoparticle) (%)	AgNC (silver nanocomposite) (%)
Z-average size (nm)	138.8	244
Peak 1 mean (nm) area (%)	210.6 (92.2)	138.6 (94.6)
Peak 2 mean (nm) area (%)	21.2 (5.16)	18.0 (5.3)
Polydispersity index	0.403	0.218

Table 2: Zeta potential parameters of AgNPs and AgNC nanocomposite

Parameter	AgNPs (silver nanoparticle)	AgNC (Silver nanocomposite)
Mean zeta potential (mV)	−38.64	−61.10
Zeta peak 1 (mV)	−76.87	−71.54
Zeta peak 2 (mV)	−39.83	−54.49
Conductivity (mS/cm)	1.781	0.437
Wall zeta potential (mV)	−38.17	−62.56
Quality factor	3.385	6.817
Temperature (°C)	25	25

Table 3: Map sum spectrum of AgNC EDX elemental analysis with relative weight and atomic proportion

Element	Weight %	Atomic %
C	44.26	60.24
O	32.33	33.03
Na	1.29	0.91
Al	1.41	0.85
Si	0.13	0.08
Cl	0.88	0.41
K	3.20	1.34
Ca	1.47	0.60
Fe	0.77	0.23
Cu	1.49	0.38
Ag	12.79	1.94
Total	100.00	100.00

EDX: Energy dispersive X-ray

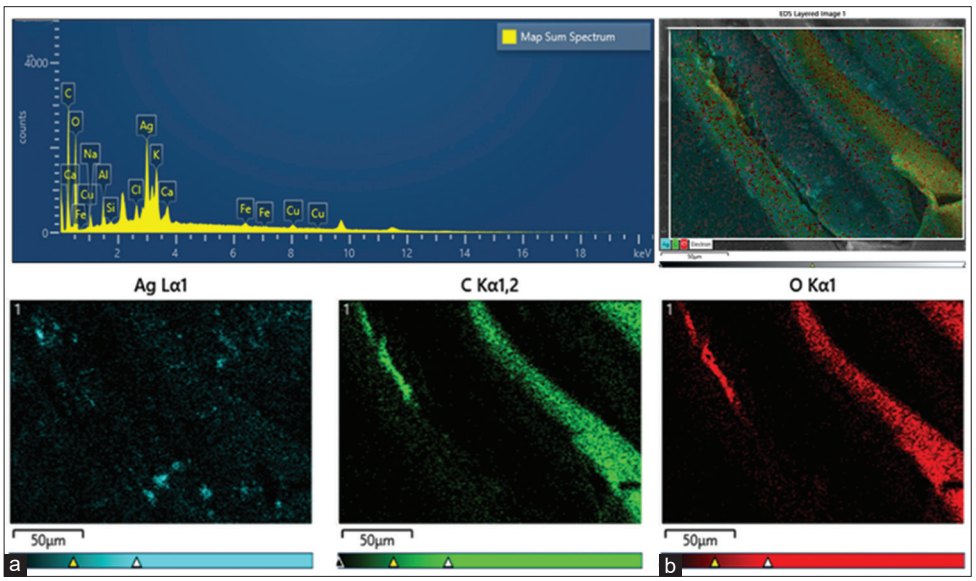

Fig. 8. Scanning electron microscopy analysis with energy-dispersive X-ray spectroscopy, (a) Shown an energy dispersive X-ray spectrum, (b) a corresponding elemental Map uniform distribution of silver (Ag, blue), carbon (C, green) and oxygen (O, red)

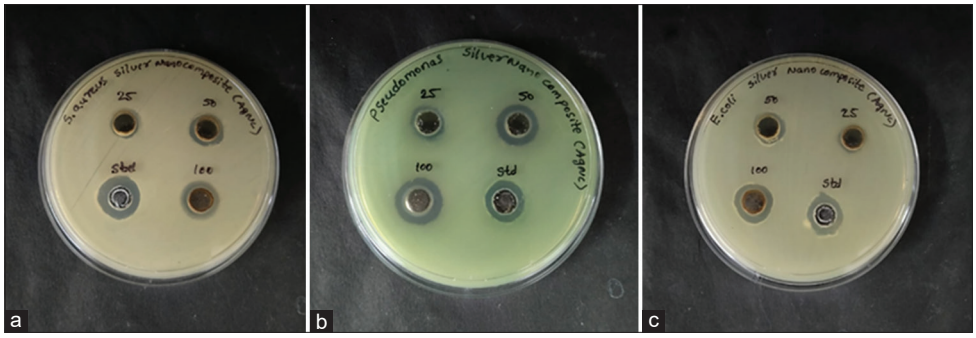

Fig. 9: Antibacterial activity of silver nanocomposite in (a) *Staphylococcus aureus*, (b) *Pseudomonas aeruginosa*, and (c) *Escherichia coli* using agar well-diffusion method

and 100 µg/mL. The zone of inhibition was measured in millimeters (mm), and the results were compared with a standard antibiotic (Fig. 9). For *S. aureus,* the zone of inhibition was 10 mm, 13 mm, and 14 mm, respectively, compared with the standard 16 mm. Against *P. aeruginosa, inhibition* zones were 12 mm, 15 mm, and 16 mm, demonstrating superior efficacy at higher concentrations compared to the standard antibiotic (15 mm). This result suggests that AgNCs may have better antibacterial activity against *P. aeruginosa.* For *E. coli*, the inhibition zones of the nanocomposite were 11 mm, 12 mm, and 16 mm, while the standard showed 14 mm; this indicates that AgNCs exhibit strong antibacterial efficacy [46,47]. The highest concentration (100 µg/mL) demonstrated a significant antibacterial activity across all bacterial strains (Fig. 10). These results correlated with previous studies, phytochemicals of *P. betel* extract alkaloids, eugenol, tannins and silver ions interact with esterase DNA, RNA, polymerase, and cell respiration play an important role in DNA intercalation acts as antibacterial agents [13,46].

Determination of MIC and MBC

The results revealed that the AgNC indicated strong growth inhibition and absence of turbidity at relatively low concentrations at 20 µg/mL for *S. aureus*, 15 µg/mL for *P. aeruginosa*, and *E. coli*. The MBC for all tested organisms was ranged between 30 and 40 µg/mL; these results demonstrate the potent antibacterial potential of biosynthesized Ag-chitosan nanocomposite (AgNC) [48].

Cytoplasmic leakage assay

The concentration-dependent cytoplasmic leakage was observed in the treatment group compared with the positive control; higher concentrations exhibited more significant effects. *P. aeruginosa* and *E. coli* showed higher levels of cytoplasmic leakage compared to *S. aureus* (Fig. 11). Increased cytoplasmic leakage in *P. aeruginosa, E. coli* indicates the potent antibacterial effect of the AgNC, possibly due to the interaction of AgNC with bacterial proteins and DNA, leading to oxidative stress and cellular damage [10]. The interaction of AgNC with bacterial cell walls and the generation of reactive oxygen species (ROS) likely contribute to bacterial membrane disruption and cell death.

Protein leakage assay

The protein leakage from cells was increased along with an increase in AgNC concentration, compared with standard (Fig. 12). A significant difference was observed with all concentrations in *P. aeruginosa* and *E. coli.* Maximum protein leakage was noted in 100 µg/mL. Moreover, Tannins are bioactive compounds that can coagulate bacterial protoplasm, cause proteins to precipitate and bind to one another, and inhibit the development of bacterial cell walls [8,33].

Ani-biofilm activity

The results indicate a dose-dependent inhibition of biofilm formation; the control exhibited the highest biofilm mass, while treatment groups with increasing concentration significantly reduced biofilm formation (Fig. 13). Significant anti-biofilm activity was observed at higher concentrations (50–100 µg/mL), with *S. aureus* and *E. coli* showing

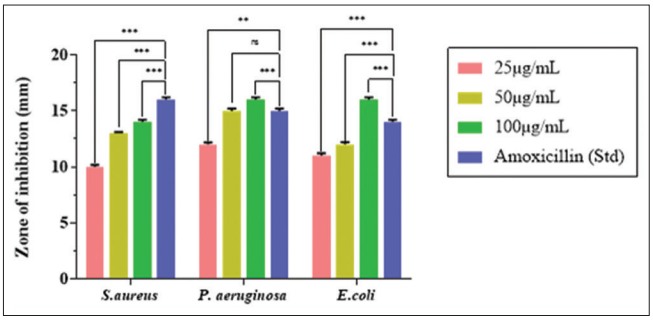

Fig. 10: Antibacterial activity of betel stem silver nanocomposite. Results were presented in mean±standard deviation, n=3(triplicates), ** p<0.01, ***p<0.001, nsp>0.05=not significant

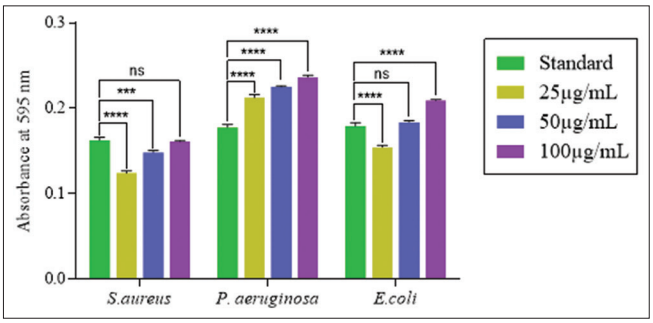

Fig. 11: Cytoplasmic leakage analysis of silver nanocomposite. Results were presented in mean±standard deviation, n=3 (triplicates), ***p<0.001, ****p<0.0001, and ns p>0.05

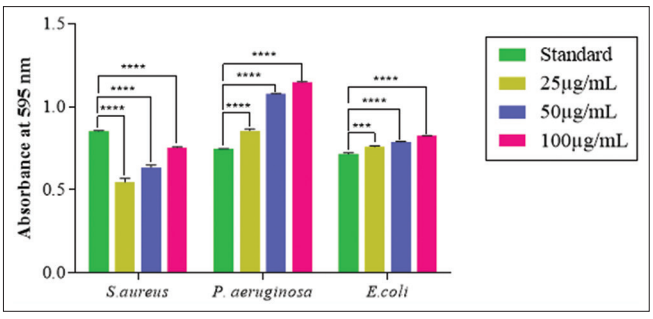

Fig. 12: Protein leakage analysis of silver nanocomposite using Bradford reagent assay. Data presented in mean±standard deviation, n=3 (triplicates), two-way analysis of variance statistical significance was shown with asterisk (*),*p<0.001, ****p<0.0001, and ns p>0.05**

the strongest response. These findings align with earlier research that has reported antibiofilm activity of silver-based NPs and silver

nanocomposites that possess strong antibiofilm activity by disrupting bacterial cell walls and generating ROS [38,49]. Furthermore, higher silver concentration leads to enhanced penetration into the cell walls and bacterial membrane damage [50,51]. Further research is needed to explore the mechanistic pathways of AgNC exerting biofilm-inhibitory effects.

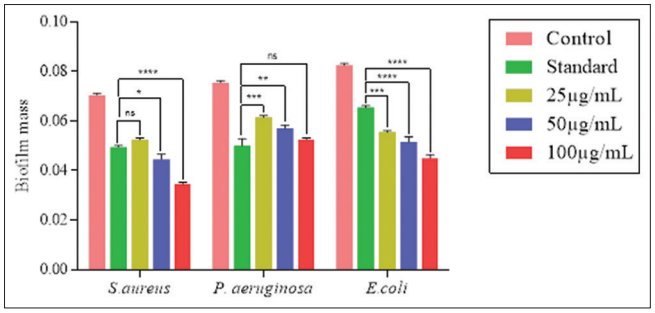

Fig. 13: Anti-biofilm activity of silver nanocomposite. Values are expressed as the mean and standard deviation error bars of n=3 (replicated), statistical significance were presented with asterisk (*), *p<0.05, **p<0.01, ***p<0.001, ****p<0.0001, and ns p>0.05

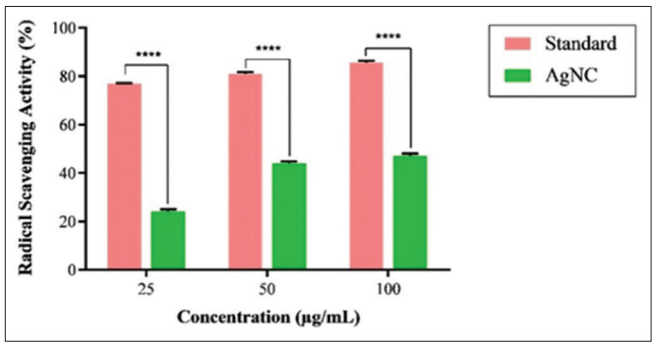

Fig. 14: Anti-oxidant activity of silver nanocomposite using diphenyl-2-picrylhydrazyl assay. Bar graph was presented with mean percentage and standard deviation error bars, n=3 (replicated), statistical significance was presented with asterisk (*), ****p<0.0001

Antioxidant assay

The DPPH assay showed concentration-dependent free radical inhibition activity by AgNC NPs (Fig. 14). The percentage of antioxidant activity (24, 47, 44) increased with concentrations from 25, 50, and 100 µg/mL, which was lower compared to the standard. This was supported by Sonphakdi *et al*., who reported that phenolic compounds donate electrons to other molecules and exhibit antioxidant activity [7]. These findings highlight the effectiveness of AgNC in reducing oxidative stress, which could be beneficial for biomedical and pharmaceutical applications.

Anti-inflammatory assay

The anti-inflammatory property of AgNC in EA and BSA assays confirmed that it effectively inhibits protein denaturation, a key factor in inflammation. The percentage of inhibition was increased with an increase in concentration (Fig. 15), with the maximum inhibition observed at 100 µg/mL (67%, 92%). The EA assay showed that the inhibition was nearly equivalent to the standard drug. Similarly, the BSA was slightly less than the standard drug. These findings highlight the strong anti-inflammatory potential of AgNC, closely matching the effectiveness of the standard drug [32]. Moreover, reinforce the potential of AgNC in the management of inflammation. The bioactive components phenol compounds, flavonoids, and terpenoids are responsible for anti-inflammatory activity [6].

Anticancer activity

Cytotoxicity assay (MTT)

In *vitro*, cytotoxicity activity results of AgNC in A549, HEK, and HeLa cell lines were presented as a mean percentage of viability (Fig. 16). AgNC exhibited dose-dependent cytotoxicity, but its higher IC_{50} suggests less potential than cisplatin in both cancer cell lines (Table 4). The greater cytotoxic effect was observed in A549 cells, suggesting higher susceptibility compared to HeLa cells with AgNC. Furthermore, we found less cytotoxicity towards HEK cell lines compared to the standard drug cisplatin [52,53]. The results suggest that AgNC has

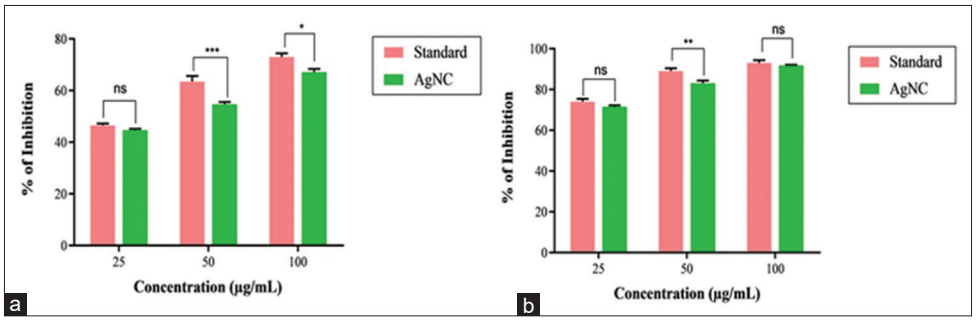

Fig. 15: Anti-inflammatory assay of silver nanocomposite, through the (a) egg albumin and (b) bovine serum albumin, bar graph was presented with mean percentage and standard deviation error bars, n=3 (replicated), *p<0.05, **p<0.01, ***p<0.001, ****p<0.0001, and ns p>0.05

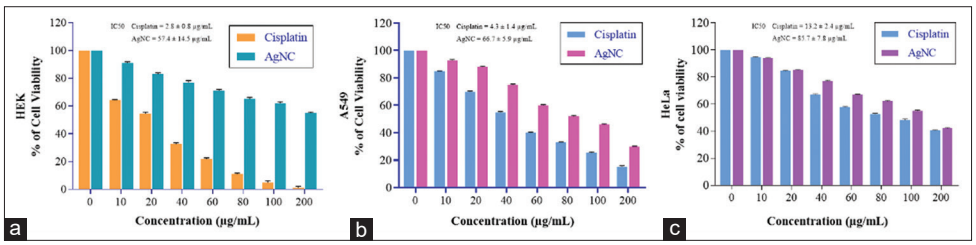

Fig. 16: Effect of *Piper betel* silver nanocomposite and cisplatin at different concentrations in (a) human embryonic kidney, (b) A549, and (c) Henrietta Lacks cell lines. Data represented in graph as viability mean with standard deviation error bars, n=3

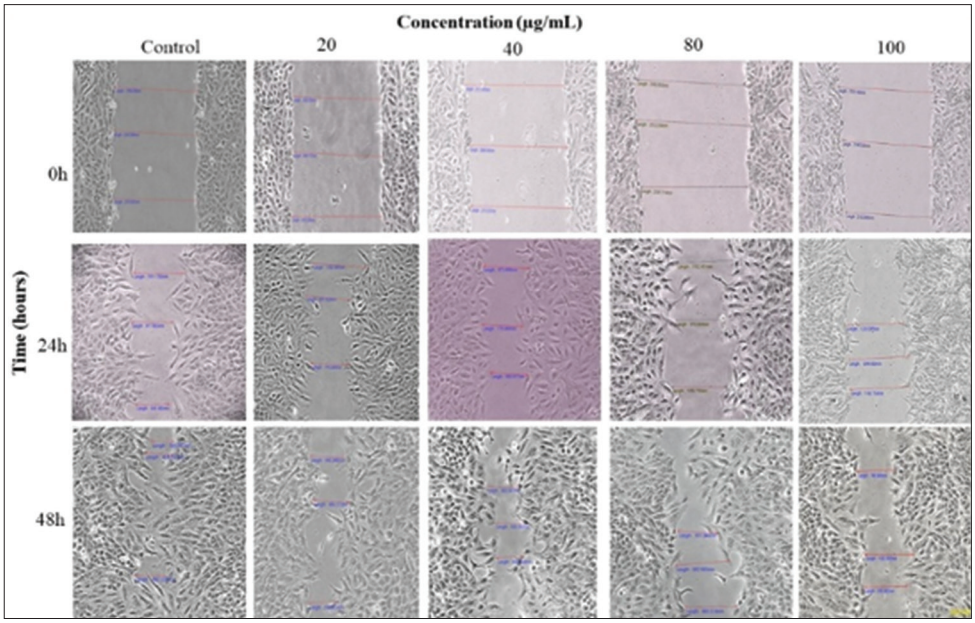

Fig. 17: Effect of different concentrations of silver nanocomposite in A549 cell lines migration at 0, 24, and 48 h

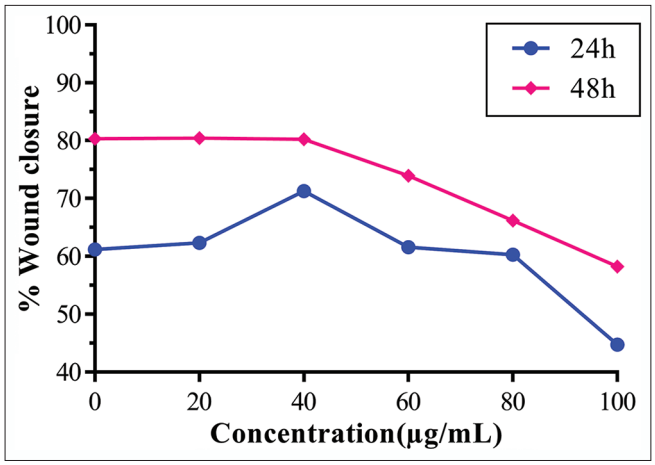

Fig. 18: Effect of silver nanocomposite on wound closure of A549 cell lines at 24 and 48 h, mean of wound closure are was plotted in graph as percentage

potent anticancer activity but requires a higher concentration, and the potential of AgNC is possibly enhanced with the combination of other drugs for its effectiveness [22,54]. These results were correlated with previous research conducted in *P. betel* AgNPs, conjugation of AgNPs with chitosan [55-57]. Several studies have reported that cytotoxicity depends on several factors, such as the particle size of NPs and the type of cell line [58]. As a result, more investigation is required to use enhance the AgNC as an effective cancer therapy medicine.

Cell migration (scratch wound healing) assay

The cell migration assay exhibited significant differences at various concentrations across different time points (0 h, 24 h, 48 h) and drug concentrations (20, 40, 80, and 100 µg/mL) compared to the control group (Fig. 17). Cell migration reduction was observed at 24 h compared to 0 h. The significant decline of cell migration at 48 h indicates a substantial inhibition at 48 h. Overall, the results suggest a time-dependent decrease in cell migration from 0 to 48 h (Fig. 18), with an increasing concentration of AgNC. Notably, a significant inhibition was observed at 80 µg/mL (**p=0.001) and 100 µg/mL (***p<0.0001) [52].

Table 4: IC_{50} values (µg/mL) of cisplatin and AgNCin HEK, A549, and HeLa cell lines

Cell line	Cisplatin (Mean±SD)	AgNC (Mean±SD)
A549	4.3±1.4	66.7±5.9
HeLa	13.2±2.4	85.7±7.8
HEK	2.8±1.0	57.4±14.5

Values are expressed as mean±SD (standard deviation) from three independent experiments (n=3), units were in micrograms per milliliters (µg/mL)

CONCLUSION

In this present study, successfully synthesized chitosan-mediated silver nanocomposite (AgNC) using an aqueous *P. betel* stem extract. AgNC possessed significant antibacterial properties against pathogenic bacteria. Furthermore, it shows effective results for cytoplasmic leakage, protein leakage, antioxidant, and anti-inflammatory activity. Anticancer activity against the A549, HeLa cell lines. This study suggested that a combination of chitosan and AgNPs with green synthesis will be a good combination for developing an alternative therapeutic agent with fewer side effects and may provide a synergistic anticancer and antibacterial activity. Which may facilitate the development of a new class of antimicrobial and anticancer agents, further research is required on drug release kinetics and in *vivo* toxicity evaluation to assess the biocompatibility and safety.

Limitations

The present study demonstrates cytotoxic and antimigratory effects but does not experimentally confirm the mechanism of cell death; assays such as Annexin V/PI and ROS analysis will be included in future studies.

ACKNOWLEDGMENT

The authors would like to thank everyone who contributed to the success of this research.

AUTHOR CONTRIBUTIONS

K.N.K., N.D., and P. AK contributed to conceptualization, methodology, review, and editing. M.S., M.B.S. performed the experiments and

collected the data. M.S., K.N.K., and N.D. drafted the manuscript, T.M and N.D. supervised the study and provided technical guidance. M.S., and N.K.K. performed the statistical analysis. All authors interpreted the results and critically reviewed and revised the final manuscript.

CONFLICT OF INTEREST

The authors declare that there is no conflict of interest regarding the publication of this article.

ETHICAL APPROVAL

No animal or human studies were involved.

FUNDING

This research work is not funded by any organization.

REFERENCES

1. Rai M, Pandit R, Gaikwad S, Yadav A, Gade A. Potential applications of curcumin and curcumin nanoparticles: From traditional therapeutics to modern nanomedicine. Nanotechnol Rev. 2015;4(2):161-72. doi: 10.1515/ntrev-2015-0001
2. Rajeshkumar S, Bharath LV, Geetha R. Broad spectrum antibacterial silver nanoparticle green synthesis: Characterization, and mechanism of action. In: Green Synthesis, Characterization and Applications of Nanoparticles. Netherlands: Elsevier; 2019. p. 429-44. doi: 10.1016/B978-0-08-102579-6.00018-6
3. Goswami MJ, Hati Boruah JL, Saikia R, Dutta U, Kakati D. Synthesis, antimicrobial and antioxidant bioevaluation of silver nanoparticles using leaf extract of *Sarcochlamys pulcherrima*. Next Nanotechnol. 2024;5:100063. doi: 10.1016/j.nxnano.2024.100063
4. Kanniah P, Chelliah P, Thangapandi JR, Gnanadhas G, Mahendran V, Robert M. Green synthesis of antibacterial and cytotoxic silver nanoparticles by *Piper nigrum* seed extract and development of antibacterial silver-based chitosan nanocomposite. Int J Biol Macromol. 2021;189:18-33. doi: 10.1016/j.ijbiomac.2021.08.056, PMID 34389391
5. El-Meligy MA, Abd El-Monaem EM, Eltaweil AS, Mohy-Eldin MS, Ziora ZM, Heydari A, *et al*. Recent advancements in metallic Au- and Ag-based chitosan nanocomposite derivatives for enhanced anticancer drug delivery. Molecules. 2024;29(10):2393. doi: 10.3390/molecules29102393, PMID 38792255
6. Singh T, Singh P, Pandey VK, Singh R, Dar AH. A literature review on bioactive properties of betel leaf (*Piper betel* L.) and its applications in food industry. Food Chem Adv. 2023;3:100536. doi: 10.1016/j.focha.2023.100536
7. Sonphakdi T, Tani A, Payaka A, Ungcharoenwiwat P. Antibacterial and toxicity studies of phytochemicals from *Piper betle* leaf extract. J King Saud Univ Sci. 2024;36(10):103430. doi: 10.1016/j.jksus.2024.103430
8. Alven S, Aderibigbe BA. Chitosan-based scaffolds incorporated with silver nanoparticles for the treatment of infected wounds. Pharmaceutics. 2024;16(3):327. doi: 10.3390/pharmaceutics16030327, PMID 38543221
9. Sivanesan I, Gopal J, Muthu M, Shin J, Mari S, Oh J. Green synthesized chitosan/chitosan nanoforms/nanocomposites for drug delivery applications. Polymers (Basel). 2021;13(14):2256. doi: 10.3390/polym13142256, PMID 34301013
10. Biswas P, Anand U, Saha SC, Kant N, Mishra T, Masih H, *et al*. Betelvine (*Piper betle* L.): A comprehensive insight into its ethnopharmacology, phytochemistry, and pharmacological, biomedical and therapeutic attributes. J Cell Mol Med. 2022;26(11):3083-119. doi: 10.1111/jcmm.17323, PMID 35502487
11. Kalaivani R, Maruthupandy M, Muneeswaran T, Hameedha Beevi A, Anand M, Ramakritinan CM, *et al*. Synthesis of chitosan-mediated silver nanoparticles (Ag NPs) for potential antimicrobial applications. Front Lab Med. 2018;2(1):30-5. doi: 10.1016/j.flm.2018.04.002
12. Badawy ME, Lotfy TM, Shawir SM. Preparation and antibacterial activity of chitosan-silver nanoparticles for application in preservation of minced meat. Bull Natl Res Cent. 2019;43(1):83. doi: 10.1186/s42269-019-0124-8
13. Nguyen TT, Le TQ, Nguyen TT, Nguyen LT, Nguyen DT, Tran TV. Characterizations and antibacterial activities of passion fruit peel pectin/chitosan composite films incorporated *Piper betle* L. leaf extract for preservation of purple eggplants. Heliyon. 2022;8(8):e10096. doi: 10.1016/j.heliyon.2022.e10096, PMID 36016528
14. Tamboli M, Tamboli N. Exploration of *in-vitro* anti-cancer activity of *Piper betel* Linn. SSRN J. 2024;11(2):157-165. doi: 10.2139/ssrn.4854818
15. Veettil SR, Sunil EA, Mukunda A, Mohan A, John S, Pynadath MK. Anticancer effect of *Piper betle* leaf extract on KB cell lines - an *in vitro* study. Oral Maxillofac Pathol J. 2022;13(1):28-31.
16. Mohamad N, Rahman A, Sheikh Abdul Kadir SH. Hydroxychavicol as a potential anticancer agent [review]. Oncol Lett. 2022;5;25(1):34. doi: 10.3892/ol.2022.13620
17. Yoonus J, Resmi R, Beena B. Greener nanoscience: *Piper betel* leaf extract mediated synthesis of CaO nanoparticles and evaluation of its antibacterial and anticancer activity. Mater Today Proc. 2021;41:535-40. doi: 10.1016/j.matpr.2020.05.246
18. Tagrida M, Nilsuwan K, Gulzar S, Prodpran T, Benjakul S. Fish gelatin/chitosan blend films incorporated with betel (*Piper betle* L.) leaf ethanolic extracts: Characteristics, antioxidant and antimicrobial properties. Food Hydrocoll. 2023;137:108316. doi: 10.1016/j.foodhyd.2022.108316
19. El-Naggar NE, Shiha AM, Mahrous H, Mohammed AB. Green synthesis of chitosan nanoparticles, optimization, characterization and antibacterial efficacy against multi drug resistant biofilm-forming *Acinetobacter baumannii*. Sci Rep. 2022;12(1):19869. doi: 10.1038/s41598-022-24303-5, PMID 36400832
20. Charirak P, Prajantasan R, Premprayoon K, Srikacha N, Ratananikom K. In vitro antibacterial activity and mode of action of *Piper betle* extracts against soft rot disease-causing bacteria. Scientifica. 2023;2023(1):5806841. doi: 10.1155/2023/5806841, PMID 37766936
21. Sumithra M, Aparna Y, Raghavendra Rao P. Morphological growth study of extended branches of silver nanodendrites using *Piper betel* leaf extract. Mater Today Proc. 2023;92:671-8. doi: 10.1016/j.matpr.2023.04.176
22. Li CX, Elhassan GO, Abdoun SA, Khan RA, Goyal M, Bansal M, *et al*. Ultra-fast synthesis of curcumin-loaded silver nanoparticles: Improved physicochemical properties for drug delivery. Int J App Pharm. 2025;17(1):216-23. doi: 10.22159/ijap.2025v17i1.52647
23. Mirda E, Idroes R, Khairan K, Tallei TE, Ramli M, Earlia N, *et al*. Synthesis of chitosan-silver nanoparticle composite spheres and their antimicrobial activities. Polymers (Basel). 2021;13(22):3990. doi: 10.3390/polym13223990, PMID 34833288
24. Arif D, Niazi MB, Ul-Haq N, Anwar MN, Hashmi E. Preparation of antibacterial cotton fabric using chitosan-silver nanoparticles. Fibers Polym. 2015;16(7):1519-26. doi: 10.1007/s12221-015-5245-6
25. Malarkodi C, Rajeshkumar S, Annadurai G. Detection of environmentally hazardous pesticide in fruit and vegetable samples using gold nanoparticles. Food Control. 2017;80:11-8. doi: 10.1016/j.foodcont.2017.04.023
26. Balouiri M, Sadiki M, Ibnsouda SK. Methods for *in vitro* evaluating antimicrobial activity: A review. J Pharm Anal. 2016;6(2):71-9. doi: 10.1016/j.jpha.2015.11.005, PMID 29403965
27. Kakian F, Mirzaei E, Moattari A, Takallu S, Bazargani A. Determining the cytotoxicity of the minimum inhibitory concentration (MIC) of silver and zinc oxide nanoparticles in ESBL and carbapenemase producing *Proteus mirabilis* isolated from clinical samples in Shiraz, Southwest Iran. BMC Res Notes. 2024;17(1):40. doi: 10.1186/s13104-023-06402-2, PMID 38287416
28. Topçu S, Şeker MG. *In vitro* antimicrobial effects and inactivation mechanisms of 5,8-dihydroxy-1,4-napthoquinone. Antibiotics (Basel). 2022;11(11):1537. doi: 10.3390/antibiotics11111537, PMID 36358192
29. Munusamy T, Shanmugam R. Green synthesis of copper oxide nanoparticles synthesized by *Terminalia chebula* dried fruit extract: Characterization and antibacterial action. Cureus. 2023;15(12):e50142. doi: 10.7759/cureus.50142, PMID 38186403
30. Dhanraj G, Rajeshkumar S. Anticariogenic effect of selenium nanoparticles synthesized using *Brassica oleracea*. J Nanomater. 2021;2021(1):1-9. doi: 10.1155/2021/8115585
31. Chandra S, Chatterjee P, Dey P, Bhattacharya S. Evaluation of *in vitro* anti-inflammatory activity of coffee against the denaturation of protein. Asian Pac J Trop Biomed. 2012;2(1):S178-80. doi: 10.1016/S2221-1691(12)60154-3
32. Ameena M, Arumugham IM, Ramalingam K, Rajeshkumar S. Evaluation of the anti-inflammatory, antimicrobial, antioxidant, and cytotoxic effects of chitosan thiocolchicoside-lauric acid nanogel. Cureus. 2023;15(9):e46003. doi: 10.7759/cureus.46003, PMID 37900405
33. Swidan NS, Hashem YA, Elkhatib WF, Yassien MA. Antibiofilm activity of green synthesized silver nanoparticles against biofilm

associated enterococcal urinary pathogens. Sci Rep. 2022;12(1):3869. doi: 10.1038/s41598-022-07831-y, PMID 35264654
34. Available from: https://manuals/man0019028_cyquant_mtt_cellproliferationassaykit_pi.pdf
35. Nandhini JT, Ezhilarasan D, Rajeshkumar S. An ecofriendly synthesized gold nanoparticles induces cytotoxicity via apoptosis in HEPG2 cells. Environ Toxicol. 2021;36(1):24-32. doi: 10.1002/tox.23007, PMID 32794643
36. Grada A, Otero-Vinas M, Prieto-Castrillo F, Obagi Z, Falanga V. Research techniques made simple: Analysis of collective cell migration using the wound healing assay. J Invest Dermatol. 2017;137(2):e11-6. doi: 10.1016/j.jid.2016.11.020, PMID 28110712
37. Ermawati DE, Yugatama A, Ramadhani BR, Pertiwi I, Rosikhoh A, Novachiria SR. Stability and antibacterial activity test of nanosilver biosynthetic hydrogel. Int J App Pharm. 2022;14(2):221-6. doi: 10.22159/ijap.2022v14i2.43584
38. Amar AA, Putra ED, Satria D, Sitorus P, Lee HL, Waruwu SB, *et al*. Biosynthesis and biological activity of silver nanoparticles from *Zanthoxylum acanthopodium* fruits. S Afr J Chem Eng. 2025;52:271-81. doi: 10.1016/j.sajce.2025.03.002
39. Wang LS, Wang CY, Yang CH, Hsieh CL, Chen SY, Shen CY, *et al*. Synthesis and anti-fungal effect of silver nanoparticles-chitosan composite particles. Int J Nanomedicine. 2015;10:2685-96. doi: 10.2147/IJN.S77410, PMID 25878501
40. Govindan S, Nivethaa EA, Saravanan R, Narayanan V, Stephen A. Synthesis and characterization of chitosan-silver nanocomposite. Appl Nanosci. 2012;2(3):299-303. doi: 10.1007/s13204-012-0109-5
41. Kulikouskaya V, Hileuskaya K, Kraskouski A, Kozerozhets I, Stepanova E, Kuzminski I, *et al*. Chitosan-capped silver nanoparticles: A comprehensive study of polymer molecular weight effect on the reaction kinetic, physicochemical properties, and synergetic antibacterial potential. SPE Polym. 2022;3(2):77-90. doi: 10.1002/pls2.10069
42. Saadh MJ. Silver nanoparticles inhibit infectious bronchitis virus replication. Int J App Pharm. 2023;15(6):163-6. doi: 10.22159/ijap.2023v15i6.48963
43. Mannopantar SR, Bendigeri HH, Kulkarni VK, Patil VS, Manjunatha DH, Kalasad MN. Preparation of colloidal Ag nanoparticles. Mater Today Proc. 2022;60:1156-9. doi: 10.1016/j.matpr.2022.03.152
44. Jalab J, Abdelwahed W, Kitaz A, Al-Kayali R. Green synthesis of silver nanoparticles using aqueous extract of *Acacia cyanophylla* and its antibacterial activity. Heliyon. 2021;7(9):e08033. doi: 10.1016/j.heliyon.2021.e08033, PMID 34611564
45. Ogungbesan SO, Buxaderas E, Adedokun RA, Moglie Y, Grijalvo S, García MT, *et al*. Synthesis and characterization of chitosan-silver nanocomposite film: antibacterial and cytotoxicity study. ChemistrySelect. 2024;9(42):e202404909. doi: 10.1002/slct.202404909
46. Sherif HH, Khalil SK, Hegazi AG, Khalil WA, Moharram MA. Factors affecting the antibacterial activity of chitosan-silver nanocomposite. IET Nanobiotechnol. 2017;11(6):731-7. doi: 10.1049/iet-nbt.2016.0249
47. Vas NV, Jain RK, Kaliaperumal K. An *in-vitro* analysis of the mechanical and anti-bacterial properties of betel leaf extract with chitosan coating on orthodontic aligners. Pesqui Bras Odontopediatr Clin Integr. 2024 Nov;25:e230243.
48. dos Santos EM, Martins CC, de Oliveira Santos JV, da Silva WR, Silva SB, Pelagio-Flores MA, *et al*. Silver nanoparticles-chitosan composites activity against resistant bacteria: Tolerance and biofilm inhibition. J Nanopart Res. 2021;23(8):196. doi: 10.1007/s11051-021-05314-1, PMID 34456615
49. Xu J, Li Y, Wang H, Zhu M, Feng W, Liang G. Enhanced antibacterial and anti-biofilm activities of antimicrobial peptides modified silver nanoparticles. Int J Nanomedicine. 2021;16:4831-46. doi: 10.2147/IJN.S315839, PMID 34295158
50. Bruna T, Maldonado-Bravo F, Jara P, Caro N. Silver nanoparticles and their antibacterial applications. Int J Mol Sci. 2021;22(13):7202. doi: 10.3390/ijms22137202, PMID 34281254
51. Muneeswaran T, Maruthupandy M, Mary AS, Vennila T, Rajaram K, Ramakritinan CM, *et al*. Starch-mediated synthesis of chitosan/silver nanocomposites for antibacterial, antibiofilm and wound healing applications. J Drug Deliv Sci Technol. 2023;84:104424. doi: 10.1016/j.jddst.2023.104424
52. Hussein HS, Ngugi C, Tolo FM, Maina EN. Anticancer potential of silver nanoparticles biosynthesized using *Catharanthus roseus* leaves extract on cervical (HeLa229) cancer cell line. Sci Afr. 2024;25:e02268. doi: 10.1016/j.sciaf.2024.e02268
53. Xu G, Yu H, Shi X, Sun L, Zhou Q, Zheng D, *et al*. Cisplatin sensitivity is enhanced in non-small cell lung cancer cells by regulating epithelial-mesenchymal transition through inhibition of eukaryotic translation initiation factor 5A2. BMC Pulm Med. 2014;14(1):174. doi: 10.1186/1471-2466-14-174, PMID 25380840
54. El-Sheikh SM, Edrees N, EL-Sayed H, Khamis T, Arisha AH, Metwally MM, *et al.* Could cisplatin loading on biosynthesized silver nanoparticles improve its therapeutic efficacy on human prostate cancer cell line and reduce its *in vivo* nephrotoxic effects? Biol Trace Elem Res. 2022;200(2):582-90. doi: 10.1007/s12011-021-02677-3, PMID 33759109
55. Gopinath V, MubarakAli D, Vadivelu J, Manjunath Kamath S, Syed A, Elgorban AM. Synthesis of biocompatible chitosan-decorated silver nanoparticles biocomposites for enhanced antimicrobial and anticancer property. Process Biochem. 2020;99:348-56. doi: 10.1016/j.procbio.2020.09.011
56. Preethi R, Padma PR. Anticancer activity of silver nanobioconjugates synthesised from *Piper betle* leaves extract and its active compound eugenol. Int J Pharm Pharm Sci. 2016;8(9):201. doi: 10.22159/ijpps.2016.v8i9.12993
57. Milliana A, Sari RA, Miranda SA, Mutiah R. Evaluation of anticancer activity and mechanism of action of myricetin on HeLa, T47D, and Vero cells: Comparative analysis with cisplatin and doxorubicin. Biomed Pharmacol J. 2025;18(1):835-47. doi: 10.13005/bpj/3133
58. Zhang XF, Shen W, Gurunathan S. Silver nanoparticle-mediated cellular responses in various cell lines: An *in vitro* model. Int J Mol Sci. 2016;17(10):1603. doi: 10.3390/ijms17101603, PMID 27669221